Available online at www.sciencedirect.com
ScienceDirect
Journal of Power Sources 162 (2006) 81–93
JOURNAL OF POWER SOURCES
www.elsevier.com/locate/jpowsour

Numerical analysis of relative humidity distribution in polymer electrolyte fuel cell stack including cooling water

Gen Inoue [a,*], Takashi Yoshimoto [a], Yosuke Matsukuma [a], Masaki Minemoto [a], Hideki Itoh [b], Shigeru Tsurumaki [b]

[a] *Department of Chemical Engineering, Faculty of Engineering, Kyushu University Motooka, Nishi-ku, Fukuoka 819-0395, Japan*
[b] *Mitsubishi Heavy Industries Ltd., Kan-on-shin-machi, Nishi-ku, Hiroshima 733-8553, Japan*

Received 27 April 2006; received in revised form 3 July 2006; accepted 5 July 2006
Available online 22 August 2006

Abstract

Polymer electrolyte fuel cell (PEFC) needs to be examined relative humidity distribution and current density distribution to improve the durability. In this study, the PEFC reaction and thermal flow analysis model including the effect of cooling water was developed. Furthermore, the effects of the shape of separator channels and the flow pattern on current density distribution and relative humidity distribution were examined by this numerical analysis. As a result, it was found that the uniform current density distribution did not directly relate to the uniform humidity distribution, because the humidity distribution was complexly affected by the generated water, the water transfer between the anode and the cathode and the gas temperature. Moreover, it was confirmed that the optimal flow pattern of gas and cooling water could make the relative humidity higher and more uniform. This calculation model can help us to design the optimal separator shape and to determine the optimal operating conditions which can narrow the low humidity area and improve the cell durability.
© 2006 Elsevier B.V. All rights reserved.

Keywords: PEFC; Numerical analysis; Current density distribution; Relative humidity distribution; Cooling water

1. Introduction

Recently, environmental pollution and destruction of ecosystem has been getting worse because of mass consumption of fossil fuels such as petroleum. The exhaustion of these energy resources becomes a serious problem. In order to contribute to solve these problems, fuel cells are expected to be practical use because it emits less environmental pollutant and converts more efficiently from chemical energy to electrical energy than other energy resources. Especially, polymer electrolyte fuel cell (PEFC) is expected as driving power of vehicles and stationary power supply, because it can work at low temperature and has high power density. The performance of PEFC has improved rapidly by developing the new component materials and optimizing the system. In order to spread PEFC for various uses, it is necessary to improve the durability and the cell output, and to reduce the cost. The power generated by PEFC is affected by the structure, the material and the operating conditions through the process of generation. The phenomena of mass transfer, heat transfer, catalysis, electrochemical reactions and fluid dynamics are shown only in an internal cell, and it is greatly important to understand the correlation among such complex phenomena in detail to improve and optimize the PEFC component and the system. However, these phenomena are caused regardless of the size of the area from an interface of catalyst layers to a stack, and these phenomena affect each other intricately. Therefore, it is very difficult to measure local conditions accurately by experiments, and very few researchers examine that.

In recent years, a numerical analysis method has been used to examine that. Nguyen and White [1], and Yi and Nguyen [2] developed the heat and water transport models (2D) which accounted for various operating conditions and hydration of the membrane. On the other hand, it is thought that the analysis with the computational fluid dynamics (CFD) is important to calculate the transport phenomena in detail, and such kinds of studies have been increasing recently. Um et al. [3] and Wang et al. [4] have developed the two-dimensional model with CFD which included two-phase flow. Dutta et al. [5] made the

* Corresponding author. Tel.: +81 92 802 2765; fax: +81 92 802 2785.
E-mail address: ginoue@chem-eng.kyushu-u.ac.jp (G. Inoue).

0378-7753/$ – see front matter © 2006 Elsevier B.V. All rights reserved.
doi:10.1016/j.jpowsour.2006.07.017

Nomenclature

b_c	condensation rate constant (s^{-1})
C_j	molar concentration of species j ($mol\,m^{-3}$)
$C_{j(n)}$	molar concentration of species j in next channel of n direction ($mol\,m^{-3}$)
C_p	specific heat at constant pressure ($J\,kg^{-1}\,K^{-1}$)
$C^{e}_{O_2}$	oxygen concentration at catalyst layer ($mol\,m^{-3}$)
$C^{ref}_{O_2}$	reference oxygen concentration ($mol\,m^{-3}$)
D_j	diffusion coefficient of species j ($m^2\,s^{-1}$)
D^{eff}_j	effective diffusion coefficient of species j ($m^2\,s^{-1}$)
E	electromotive force (V)
$E_{\Delta H}$	heating value converted into a theoretical voltage (V)
F	Faraday's constant ($96485\,C\,mol^{-1}$)
h	heat transfer coefficient of gas ($J\,m^{-2}\,s^{-1}\,K^{-1}$)
h^w	heat transfer coefficient of cooling water ($J\,m^{-2}\,s^{-1}\,K^{-1}$)
H_{GDL}	length of GDL gas flow area (m)
ΔH_{H_2O}	evaporation enthalpy of water ($J\,mol^{-1}$)
i	current density ($A\,m^{-2}$)
i_{O_2}	oxygen exchange current density ($A\,m^{-2}$)
k	thermal conductivity of solid phase ($J\,m^{-1}\,s^{-1}\,K^{-1}$)
k_p	permeability of GDL (m^2)
k^{sep}	thermal conductivity of separator ($J\,m^{-1}\,s^{-1}\,K^{-1}$)
$l_{d,g}$	gas channel depth (m)
l_{GDL}	GDL thickness (m)
l^s	thickness of solid phase (m)
l^{sep}	separator thickness between cooling water and gas phase (m)
M_j	molecular weight of species j ($kg\,mol^{-1}$)
p	pressure in Eq. (4) (Pa)
p_n	pressure in next channel of n direction (Pa)
$P_{H_2O,sat}$	saturated vapor pressure in stream (Pa)
Q_b	all gas flow rate through GDL per unit volume to next channel (s^{-1})
$Q_{b(n)}$	flow rate through GDL per unit volume to next channel of n direction (s^{-1})
$Q_{b(n,in)}$	inflow rate through GDL per unit volume from next channel of n direction (s^{-1})
$Q_{b(n,out)}$	outflow rate through GDL per unit volume to next channel of n direction (s^{-1})
q_1	heat flux from solid phase to gas phase ($J\,m^{-2}\,s^{-1}$)
q_2	heat flux from cooling water to gas phase ($J\,m^{-2}\,s^{-1}$)
q^s_3	heat value generated by reaction ($J\,m^{-2}\,s^{-1}$)
q^s_4	heat flux from gas phase to solid phase ($J\,m^{-2}\,s^{-1}$)
q^s_5	heat flux from cooling water to solid phase ($J\,m^{-2}\,s^{-1}$)
q^s_6	latent heat value of condensation ($J\,m^{-2}\,s^{-1}$)
q^w_1	heat flux from both side gas to cooling water ($J\,m^{-2}\,s^{-1}$)
q^w_2	heat flux from solid phase to cooling water ($J\,m^{-2}\,s^{-1}$)
R	gas constant ($8.314\,J\,mol^{-1}\,K^{-1}$)
R_{rea}	all reaction rate (s^{-1})
r_j	molar flux of species j ($mol\,m^{-2}\,s^{-1}$)
R_{ohm}	resistance of proton transfer through electrolyte membrane ($\Omega\,m^2$)
Re	Reynolds number defined in Table 1
Sc	Schmitt number defined in Table 1
Sh	Sherwood number defined in Table 1
t	time (s)
T	gas phase temperature (K)
T_n	gas temperature in next channel of n direction (K)
T^s	solid phase temperature (K)
T^w	cooling water temperature (K)
U	average gas velocity in GDL of x direction ($m\,s^{-1}$)
U_T	overall heat transfer coefficient between gas and cooling water ($J\,m^{-2}\,s^{-1}\,K^{-1}$)
U^s_T	overall heat transfer coefficient between cooling water and solid phase ($J\,m^{-2}\,s^{-1}\,K^{-1}$)
v	flow velocity ($m\,s^{-1}$)
V	operation voltage (V)
w_C	channel width (m)
w_L	land width (m)
x	x direction (m)

Greek letters

α	net water transfer coefficient
α_t	transfer coefficient
β	parameter in oxygen mass transfer model shown in Table 1
γ	variable defined in Table 1 ($A\,m\,mol^{-1}$)
ε	effective porosity of GDL
λ	parameter defined in Table 1
μ	viscosity of mixture gas (Pa s)
ρ	density of mixture gas ($kg\,m^{-3}$)
ω	parameter in oxygen mass transfer model shown in Table 1

Subscripts

H_2O	water
$H_2O(l)$	liquid water
$H_2O(v)$	vapor water
j	species j
N_2	nitrogen
O_2	oxygen
x	x direction

Superscripts

a	anode
c	cathode

channel	channel
e	electrode
eff	effective
k	anode or cathode
s	solid phase
sep	separator

three-dimensional computational model based on a commercial software package, Fluent. Berning et al. [6] presented the non-isothermal and three-dimensional models, and calculated the distribution of current density and concentration in straight channels. Um and Wang [7] compared the performance of the flow in straight channels with that in interdigitated channels by the three-dimensional analysis. Berning and Djilali [8] examined the effect of porosity and thickness of gas diffusion layers in the straight channels by the three-dimensional model. These PEFC numerical analysis models contributed to the optimization of component design and the operating conditions.

PEFC needs to be improved its durability in order to commercialize this system. There are some reports concerning the durability under various operating conditions, and it was reported that degradation of MEA caused the cell voltage to reduce and the electrolyte membrane to brake. Though the degradation mechanism has not been investigated in detail yet, it is thought that the attack by peroxide radical is responsible for this degradation phenomenon, and it is reported that this degradation is accelerated under a low humidity condition [9–12]. On the basis of this experimental result, it is effective to design the optimal operating conditions and shapes which can narrow the low humidity area in order to improve the PEFC durability. In PEFC, water and heat are generated by the electrochemical reactions, and the relative humidity, which is a function of the local temperature and the vapor concentration, is not uniform. And in the case of a stack, the effect of the cooling water for heat recovery has to be considered. There are some experimental studies concerning the humidity distribution in a cell, and important results were reported in ref. [13]. On the other hand, in order to examine the humidity distribution under various conditions and with various shapes, the numerical analysis is effective from the viewpoints of cost and time.

In our past researches [14], the effects of changing the operation temperature, the humidify temperature and the hydrogen and oxygen concentration in the supplied gas on the *i–V* characteristic of a small PEFC were examined experimentally. For the

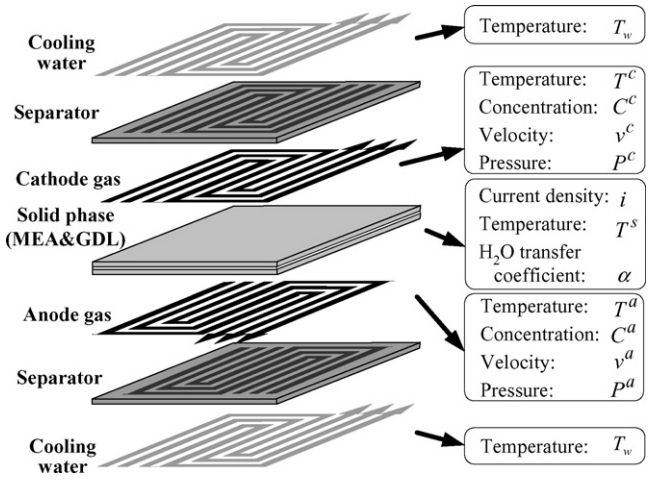

Fig. 1. Numerical analysis model including cooling water.

experiment, we developed two models: one was the PEFC reaction model that could show these influences on PEFC reaction characteristics; and the other was the PEFC reaction and flow analysis model that was combined with the thermal flow analysis. With this PEFC reaction and flow analysis model, five kinds of separators were evaluated from the viewpoints as follows: gas flow condition, uniformity of current density and temperature, reduction of pressure drop and ejection of water. In ref. [15], the simplified two-dimensional PEFC analysis model including flow and heat transfer of cooling water was made. The influence of changing the thickness of the membrane and the GDL on the cell performance was calculated. However, these previous models of ours did not include the effect of the gas flow through the gas diffusion layers. In refs. [16,17], the mass transfer and the flow in the gas diffusion layers were calculated, and the approximate model for the GDL mass transfer based on the theoretical model was developed. Next, with this model, the PEFC reaction and thermal flow analysis model which enabled us to calculate an actual-sized cell was made. The numerical analysis made it possible to examine how the separator depth and the GDL effective porosity and the GDL permeability and the flow rate of the cathode gas effected on the output performance and the current density distribution. In this study, a calculation of temperature of cooling water was combined with our past model, and PEFC reaction and flow analysis model including the effect of cooling water was developed. Furthermore, the relative humidity distribution and current density distribution were examined under various conditions with this model.

Table 1
Equations for calculation of current density and oxygen mass transfer in GDL

Current density

$$V = E - (RT/\alpha_t 2F)\ \ln[iC^{\mathrm{ref}}_{\mathrm{O_2}}/i_{\mathrm{O_2}}C^{\mathrm{e}}_{\mathrm{O_2}}] - R_{\mathrm{ohm}}i, \quad \gamma = i_{\mathrm{O_2}}/C^{\mathrm{ref}}_{\mathrm{O_2}}$$

Oxygen mass transfer in GDL

Upstream: $Sh = \beta + \lambda Re^{0.5}Sc^{0.8}$

Downstream: $Sh = \beta + \lambda(Re - \omega)^{0.5}Sc^{0.5}$

Conditions: $Sh = (i/4F)(l_{\mathrm{GDL}}/(D^{\mathrm{eff}}_{\mathrm{O_2}}(C^{\mathrm{channel}}_{\mathrm{O_2}} - C^{\mathrm{e}}_{\mathrm{O_2}})))$, $Re = l_{\mathrm{GDL}}\rho U/\mu$, $Sc = \mu/\rho D^{\mathrm{eff}}_{\mathrm{O_2}}$, $\lambda = 1/2\sqrt{l_{\mathrm{GDL}}/\pi H_{\mathrm{GDL}}}$, $D^{\mathrm{eff}}_j = \varepsilon D_j$

2. Numerical analysis model including the effect of cooling water

2.1. Single cell model and stack model with cooling water

Fig. 1 shows a single cell analysis model used in this study. As shown in this figure, the gas flow velocity, the concentration and the temperature were calculated in the gas channels on the anode and the cathode. And it was assumed that the temperature distribution of MEA and GDL were the same as each other and they were unified, and the temperature and the current density were calculated in a unified part. (This unified part is described as a solid phase from now on.) In this model, the temperature distribution of cooling water flowing behind a separator was calculated with the heat transfer among the anode gas, the cathode gas, the solid phase and the cooling water. Fig. 2 shows a stack and cooling water model. The cooling water flows among each cell. The heat of overvoltage is conducted to the cooling water through the anode gas, the cathode gas and the MEA. The cooling water is heated at an outlet, and this warmed water is utilized for cogeneration in the case of a stationary PEFC system. In order to calculate the heat balance of cooling water, the data of the temperature distribution of adjoining cells is needed. However, it is difficult to calculate the temperature distribution of all cells and the cooling water in a stack composed of about 100–200 cells, so the inlet condition and the internal condition are assumed to be equal to the adjoining cells with each other in this study. In Fig. 2, the cell A and the cell B are the same as each other, and the heat balance between the cooling water and a cell were virtually treated as periodic condition. It is thought that this hypothesis is effective at the center of a stack which consists of many layered cells, and this study examines the center of a stack. The periodic condition at the both ends of a stack is inappropriate, and so the model improving heat balance is needed in the next study.

2.2. Hypotheses and basic equations of this study model

The governing equations in this simulation were derived from the following assumptions:

1. The gas flow rate at the inlet in each channel is uniform.

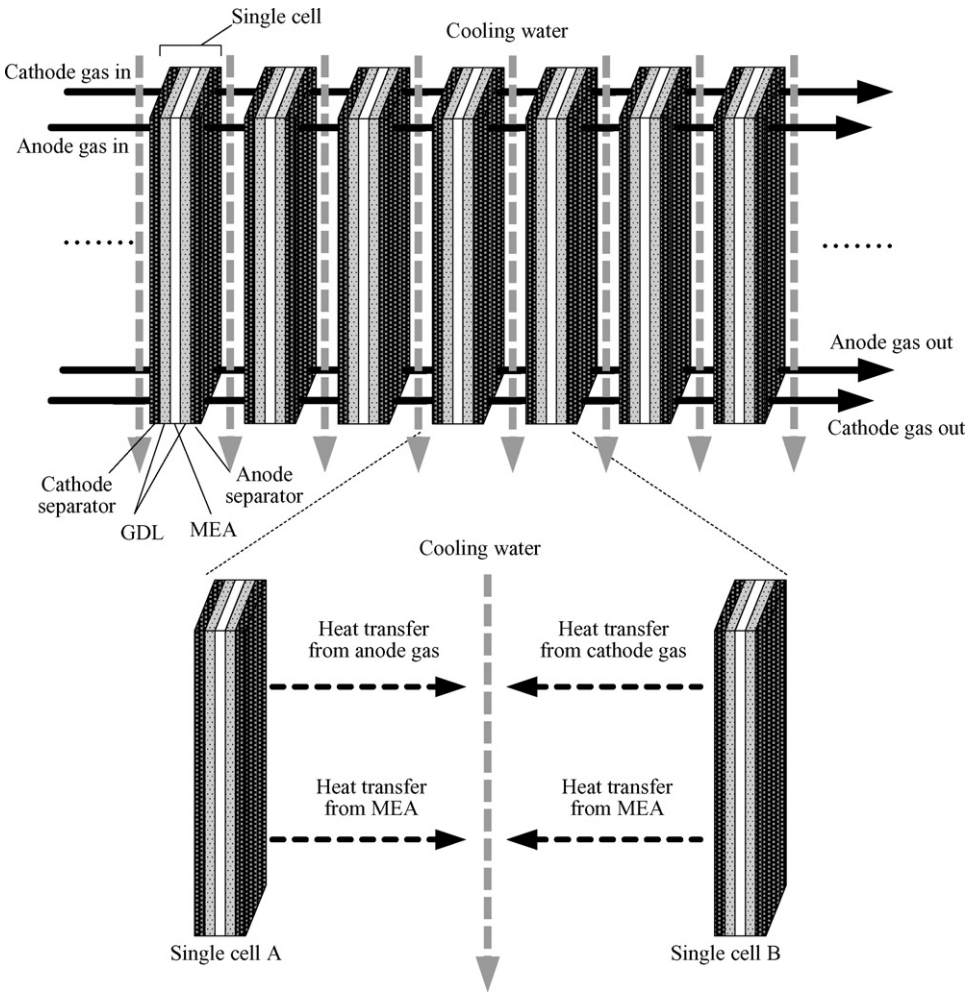

Fig. 2. Stack and cooling water model in a numerical analysis.

2. The volume of liquid water is ignored and the water moves with gas.
3. The reduction of the reacting areas caused by flooding of electrodes is ignored, and it is also ignored that liquid water prevents the diffusion.
4. Fluid is incompressible Newtonian fluid and ideal gas. The flow condition is laminar flow, and the gas properties are constant.
5. The heat transfer between separators and gas is ignored. But the heat transfer among gas phase, solid phase and cooling water is included.
6. The cell voltage is uniform and constant.
7. Only the resistance overvoltage and the water transfer in membrane include the influence of temperature.
8. In membrane, ionic conductivity, electroosmosis coefficient and water effective diffusion coefficient that depend on membrane humidity are determined by the water activity in an anode side.
9. The crossover gas through membrane is disregarded.
10. The permeability of GDL is constant and uniform.

In this study, the one-dimensional analysis as plug flow in each channel was available on the assumption that the distribution of the gas flow rate at the inlet was uniform. Though the separator shape was a two-dimensional structure to the direction of membrane surfaces, the quasi-two-dimensional analysis model could be applied on the definition that the direction from the inlet to the outlet was a positive x direction in each serpentine channel. As a result, the equations were simplified and it took less time to calculate. However, in the case of the calculations of the temperature distribution on the solid phase, it was calculated by the two-dimensional analysis model. In other studies [18,19], it was reported that supplied gas flowed through GDL which was porous media, and that the distribution of gas flow rate in channels was not uniform. In our past studies [16,17], we developed the analysis model including the effect of gas flow through GDL on cell performance. In order to calculate the gas flow rate that flowed to the next channel through GDL, pressure distribution was calculated by the two-dimensional analysis. Moreover, the following two terms in gas channels were ignored to simplify the calculations; the heat conduction term in the energy balance equations; and the diffusion term in the mass balance equations. In the calculations, as the relationship between relative humidity and the decreasing rate of cell voltage was unknown, the internal condition of a cell was calculated without degradation of MEA.

The equation of continuity is shown by the following equation,

$$\frac{\partial v^{\mathrm{k}}}{\partial x} = -R^{\mathrm{k}}_{\mathrm{rea}} - Q^{\mathrm{k}}_{b} \tag{1}$$

where v is the velocity of mixed gas, x the distance along a gas flow channel, R_{rea} all reaction rate, Q_b all gas flow rate through GDL per unit volume to the next channel and the superscript k is the anode side or the cathode side. R_{rea} is calculated by the following equation.

$$R^{\mathrm{k}}_{\mathrm{rea}} = \frac{1}{l^{\mathrm{k}}_{\mathrm{d,g}}\rho^{\mathrm{k}}}\sum_{j} M_j r^{\mathrm{k}}_{j} \tag{2}$$

where $l_{\mathrm{d,g}}$ is the depth of gas channels, ρ the density of mixed gas, M_j the molecular weight of the chemical species j and r_j is the reaction or condensation rate per unit area of the chemical species j. Q_b is calculated by the following equation,

$$Q^{\mathrm{k}}_{b} = \sum_{n} Q^{\mathrm{k}}_{b(n)} \tag{3}$$

where $Q^{\mathrm{k}}_{b(n)}$ is the gas flow rate through GDL to the n direction.

The equation of motion is shown by the following equation,

$$\rho^{\mathrm{k}}\frac{\mathrm{D}v^{\mathrm{k}}}{\mathrm{D}t} = -\nabla p^{\mathrm{k}} + \rho^{\mathrm{k}} v^{\mathrm{k}}(R^{\mathrm{k}}_{\mathrm{rea}} + Q^{\mathrm{k}}_{b}) - 12\mu^{\mathrm{k}}\left(\frac{1}{(l^{\mathrm{k}}_{\mathrm{d,g}})^2} + \frac{1}{(w^{\mathrm{k}}_{\mathrm{C}})^2}\right) v^{\mathrm{k}} \tag{4}$$

where p is the pressure, μ the gas viscosity, w_{C} the width of gas channel and the operator D/Dt is the substantial time derivative that is shown by the following equation.

$$\frac{\mathrm{D}v^{\mathrm{k}}}{\mathrm{D}t} = \frac{\partial v^{\mathrm{k}}}{\partial t} + v^{\mathrm{k}}\frac{\partial v^{\mathrm{k}}}{\partial x} \tag{5}$$

The viscous term in Eq. (4) is derived from the Hele–Show model. This term includes the effect of the viscous drag between two pairs of facing walls in a channel.

The equation of the chemical species j is shown by the following equation,

$$\frac{\mathrm{D}C^{\mathrm{k}}_{j}}{\mathrm{D}t} = -\frac{r^{\mathrm{k}}_{j}}{l^{\mathrm{k}}_{\mathrm{d,g}}} + C^{\mathrm{k}}_{j}(R^{\mathrm{k}}_{\mathrm{rea}} + Q^{\mathrm{k}}_{b}) + \sum_{n} C^{\mathrm{k}}_{j(n)} Q^{\mathrm{k}}_{b(n,\mathrm{in})} - \sum_{n} C^{\mathrm{k}}_{j} Q^{\mathrm{k}}_{b(n,\mathrm{out})} \tag{6}$$

where C_j is the concentration of the chemical species j, $C_{j(n)}$ the concentration of the chemical species j at the next channel to the n direction, $Q_{b(n,\mathrm{in})}$ the gas flow rate through GDL from the n direction adjoining channels to this point and $Q_{b(n,\mathrm{out})}$ is the gas flow rate through GDL from this point to the n direction adjoining channels. The equations of the following eight chemical species are derived: $C^{\mathrm{a}}_{\mathrm{H_2}}$, $C^{\mathrm{a}}_{\mathrm{N_2}}$, $C^{\mathrm{a}}_{\mathrm{H_2O(v)}}$, $C^{\mathrm{a}}_{\mathrm{H_2O(l)}}$, $C^{\mathrm{c}}_{\mathrm{O_2}}$, $C^{\mathrm{c}}_{\mathrm{N_2}}$, $C^{\mathrm{c}}_{\mathrm{H_2O(v)}}$, $C^{\mathrm{c}}_{\mathrm{H_2O(l)}}$ that are hydrogen, oxygen, nitrogen, vapor and condensed water in anode and cathode channels.

The equations of energy are shown by the following equations,

$$\text{(Gas)}\quad \frac{\mathrm{D}T^{\mathrm{k}}}{\mathrm{D}t} = \frac{q^{\mathrm{k}}_{1} + q^{\mathrm{k}}_{2}}{\rho^{\mathrm{k}} C^{\mathrm{k}}_{p} l^{\mathrm{k}}_{\mathrm{d,g}}} + T^{\mathrm{k}}(R^{\mathrm{k}}_{\mathrm{rea}} + Q^{\mathrm{k}}_{b}) + \sum_{n} T^{\mathrm{k}}_{n} Q^{\mathrm{k}}_{b(n,\mathrm{in})} - \sum_{n} T^{\mathrm{k}} Q^{\mathrm{k}}_{b(n,\mathrm{out})} \tag{7}$$

$$\text{(Solid)}\quad \rho^{\mathrm{s}} C_p^{\mathrm{s}} \frac{\partial T^{\mathrm{s}}}{\partial t} = k^{\mathrm{s}} \nabla^2 T^{\mathrm{s}} + \frac{q_3^{\mathrm{s}} + q_4^{\mathrm{s}} + q_5^{\mathrm{s}} + q_6^{\mathrm{s}}}{l^{\mathrm{s}}} \tag{8}$$

$$\text{(Cooling water)}\quad \frac{\mathrm{D}T^{\mathrm{w}}}{\mathrm{D}t} = \frac{q_1^{\mathrm{w}} + q_2^{\mathrm{w}}}{\rho^{\mathrm{w}} C_p^{\mathrm{w}} l^{\mathrm{w}}} \tag{9}$$

In the energy equation of gas, C_p is the specific heat, T the temperature and q_1 and q_2 are the heat fluxes from the solid phase and the cooling water, respectively. T_n is the gas temperature in the next channel to the n direction. In the equation of solid phase, k is the heat conductivity, l^{s} the thickness of solid phase, q_3 the heat value per unit area as a result of electrochemical reactions, q_4 and q_5 the heat fluxes from gas and cooling water, respectively, q_6 the latent heat flux of water condensation and the superscript s is the solid phase. In the equation of cooling water, l^{w} is the depth of channel in which cooling water flows and q_1^{w} and q_2^{w} are the heat fluxes from both sides of gas channels and from solid phase, respectively. These heat fluxes and heating values are shown by the following equations,

$$\begin{aligned}
q_1^{\mathrm{k}} &= h^{\mathrm{k}}(T^{\mathrm{s}} - T^{\mathrm{k}}) \\
q_2^{\mathrm{k}} &= U_{\mathrm{T}}^{\mathrm{k}}(T^{\mathrm{w}} - T^{\mathrm{k}}) \\
q_3^{\mathrm{s}} &= (E_{\Delta H} - V)i \\
q_4^{\mathrm{s}} &= h^{\mathrm{a}}(T^{\mathrm{a}} - T^{\mathrm{s}}) + h^{\mathrm{c}}(T^{\mathrm{c}} - T^{\mathrm{s}}) \\
q_5^{\mathrm{s}} &= 2U_{\mathrm{T}}^{\mathrm{s}}(T^{\mathrm{w}} - T^{\mathrm{s}}) \\
q_6^{\mathrm{s}} &= -\Delta H_{\mathrm{H_2O}}(r_{\mathrm{H_2O(l)}}^{\mathrm{a}} + r_{\mathrm{H_2O(l)}}^{\mathrm{c}}) \\
q_1^{\mathrm{w}} &= U_{\mathrm{T}}^{\mathrm{a}}(T^{\mathrm{a}} - T^{\mathrm{w}}) + U_{\mathrm{T}}^{\mathrm{c}}(T^{\mathrm{c}} - T^{\mathrm{w}}) \\
q_2^{\mathrm{w}} &= 2U_{\mathrm{T}}^{\mathrm{s}}(T^{\mathrm{s}} - T^{\mathrm{w}})
\end{aligned} \tag{10}$$

where h is the heat transfer coefficient of anode or cathode gas, $E_{\Delta H}$ the heating value converted into theoretical voltage, V the operating voltage, i the local current density, $\Delta H_{\mathrm{H_2O}}$ the evaporation enthalpy of water, $U_{\mathrm{T}}^{\mathrm{k}}$ the overall heat transfer coefficient between the anode gas or the cathode gas and the cooling water and $U_{\mathrm{T}}^{\mathrm{s}}$ is the overall heat transfer coefficient between the cooling water and the solid phase. These overall heat transfer coefficients are shown by the following equations,

$$\begin{aligned}
U_{\mathrm{T}}^{\mathrm{k}} &= \frac{1}{(1/h^{\mathrm{k}}) + (l^{\mathrm{sep}}/k^{\mathrm{sep}}) + (1/h^{\mathrm{w}})} \\
U_{\mathrm{T}}^{\mathrm{s}} &= \frac{1}{((l^{\mathrm{sep}} + l_{\mathrm{d,g}}^{\mathrm{k}})/k^{\mathrm{sep}}) + (1/h^{\mathrm{w}})}
\end{aligned} \tag{11}$$

where l^{sep} is the thickness of the separator between the cooling water and the gas phase and k^{sep} is the heat conductivity of the separators.

The reaction and condensation rates of each ingredient are shown by the following equations,

$$\begin{aligned}
r_{\mathrm{H_2}}^{\mathrm{a}} &= \frac{i}{2F} \\
r_{\mathrm{H_2O(v)}}^{\mathrm{a}} &= \alpha\frac{i}{F} + l_{\mathrm{d,g}}^{\mathrm{a}} b_{\mathrm{c}} \left(C_{\mathrm{H_2O(v)}}^{\mathrm{a}} - \frac{P_{\mathrm{H_2O,sat}}^{\mathrm{a}}}{RT^{\mathrm{a}}} \right) \\
r_{\mathrm{N_2}}^{\mathrm{a}} &= 0 \\
r_{\mathrm{H_2O(l)}}^{\mathrm{a}} &= -l_{\mathrm{d,g}}^{\mathrm{a}} b_{\mathrm{c}} \left(C_{\mathrm{H_2O(v)}}^{\mathrm{a}} - \frac{P_{\mathrm{H_2O,sat}}^{\mathrm{a}}}{RT^{\mathrm{a}}} \right) \\
r_{\mathrm{O_2}}^{\mathrm{c}} &= \frac{i}{4F} \\
r_{\mathrm{H_2O(v)}}^{\mathrm{c}} &= -(1+2\alpha)\frac{i}{2F} + l_{\mathrm{d,g}}^{\mathrm{c}} b_{\mathrm{c}} \left(C_{\mathrm{H_2O(v)}}^{\mathrm{c}} - \frac{P_{\mathrm{H_2O,sat}}^{\mathrm{c}}}{RT^{\mathrm{c}}} \right) \\
r_{\mathrm{N_2}}^{\mathrm{c}} &= 0 \\
r_{\mathrm{H_2O(l)}}^{\mathrm{c}} &= -l_{\mathrm{d,g}}^{\mathrm{c}} b_{\mathrm{c}} \left(C_{\mathrm{H_2O(v)}}^{\mathrm{c}} - \frac{P_{\mathrm{H_2O,sat}}^{\mathrm{c}}}{RT^{\mathrm{c}}} \right)
\end{aligned} \tag{12}$$

where F is the Faraday's constant, R the gas constant, $P_{\mathrm{H_2O,sat}}$ the saturated vapor pressure, α the water transfer coefficient and b_{c} is the condensation rate constant.

The gas flow rate through GDL is calculated by the following Darcy's model,

$$Q_{b(n)}^{\mathrm{k}} = \frac{k_{\mathrm{p}}}{\mu^{\mathrm{k}}} \frac{l_{\mathrm{GDL}}^{\mathrm{k}}}{l_{\mathrm{d,g}}^{\mathrm{k}} w_{\mathrm{C}}^{\mathrm{k}} w_{\mathrm{L}}^{\mathrm{k}}} (p^{\mathrm{k}} - p_n^{\mathrm{k}}) \tag{13}$$

where k_{p} is the permeability of GDL, l_{GDL} the thickness of GDL and w_{L} is the width of the land area between channels.

The current density distribution was calculated by the equation obtained in our past study [16]. The equations to calculate the current density are shown in Table 1. The approximate equation of the oxygen mass transfer rate to the electrode through GDL was obtained by the numerical analysis and the theoretical model. The equation was the function of the Reynolds number and the Schmitt number and was in proportion to the square root of the Reynolds number. In the equations shown in Table 1, it was found that the β was 0.624 and ω was 1.3 in the case that the width of a channel and the land were both 1 mm and the thickness of GDL was 300 μm. The current density was calculated by the oxygen mass transfer model and the overvoltage equations which were substituted for the following three local factors: the concentration of oxygen and hydrogen and vapor, the temperature of membrane and anode gas and cathode gas, and the gas flow velocity in GDL. The resistance of the proton transfer through electrolyte membrane was calculated by the Nguyen's equation [1]. In the calculation of current density with equations shown in Table 1, the same values as reference [16] were used.

It is thought that water moves with electroosmosis and back-diffusion in the electrolyte membrane. When one proton moves from the anode side to the cathode side, the water movement coefficient α shows the net number of water molecules moving along with protons. This is from the method by Nguyen and White [1].

The local concentration, the temperature, the flow velocity, the current density were calculated with Eqs. (1)–(13) and Table 1. The partial differential equations are solved by the finite differential method. The boundary conditions of the flow velocity, the temperature and the concentration are set as follows:

(1) The inlet boundary of gas: these variables are constant.
(2) The outlet boundary of gas: the gradients of these variables are constant.

The current density and the water transfer coefficient were calculated all over the electrode areas. Those variables were calculated until they became stationary state. The relative errors of the balance equations of mass, species and energy became less than 1% in all calculations. In this study, the gas flow rate was automatically set so that the utilization was constant to the prescribed average current density, and the flow rate of cooling water was automatically set so that the temperature at the outlet was constant.

Table 2
Operation condition and shape of cell

Pressure (MPa)	0.1
Inlet gas temperature (°C)	70
Inlet cooling water temperature (°C)	70
Outlet cooling water temperature (°C)	75
Humidify temperature (°C)	65
Inlet gas composition	
Anode	H_2:N_2 = 75:25
Cathode	O_2:N_2 = 21:79
H_2 utilization (%)	70
O_2 utilization (%)	40
Thickness of membrane (μm)	30
Size of catalyst layer (cm^2)	225
GDL thickness (μm)	300
Channel width (mm)	1
Channel depth (mm)	1
Land width (mm)	1
GDL permeability (m^2)	2.5×10^{-11}
Electromotive force (V)	1.23
Average current density ($A\,cm^{-2}$)	0.45

3. Results and discussions

The calculation conditions are shown in Table 2. Assuming that the influence of the changes of the gas composition on the physical property is very little, the physical properties were treated to be constant. The shapes of the gas channels are shown in Fig. 3. The electrode area is 225 cm^2 (a square, 15 cm on a side), and the widths of the channels and the land are both 1 mm. A is an ordinary serpentine separator, B is a distributed serpentine separator and both separators have 25 channels. The shape of the cooling water channels is the same as that of anode gas channels or cathode gas channels. Fig. 4 shows the flow pattern of the gas and the cooling water and Table 3 shows the combination of separator shape and flow pattern. In an actual PEFC stack, as the position of the manifold is restricted, it is difficult to set an inlet (or an outlet) of anode and cathode at the same position with each other. Accordingly, these positions were set at the symmetric position to each other in this study. The simulations were carried out under 16 conditions about the flow pattern of the gas and the cooling water, and it took 4 h per one calculation by penitum4® 3.2 GHz PC.

Fig. 5 shows the cell voltage and the average relative humidity of the anode and the cathode on each condition. In this figure, it was found that the cell voltage was almost equal to that in each condition. The average humidity of the counter gas flow (nos. 3, 4, 7, 8, 11, 12, 15 and 16) was about 5% higher than that of the parallel gas flow (nos. 1, 2, 5, 6, 9, 10, 13 and 14) in both cases of the anode and the cathode. Since the average current density and the amount of generated water were constant, it was thought that this difference was caused by the current density distribution, the water balance between the anode and the cathode and the temperature distribution.

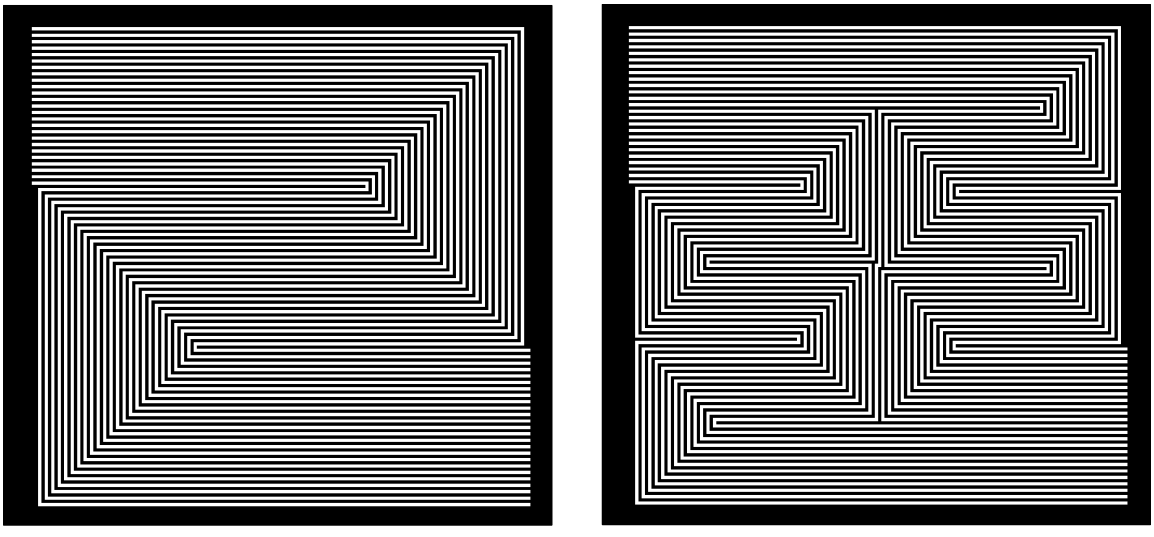

(A) (B)

Fig. 3. Separator shape: (A) is the ordinary serpentine separator with 25 channels and (B) is the distributed serpentine separator with 25 channels.

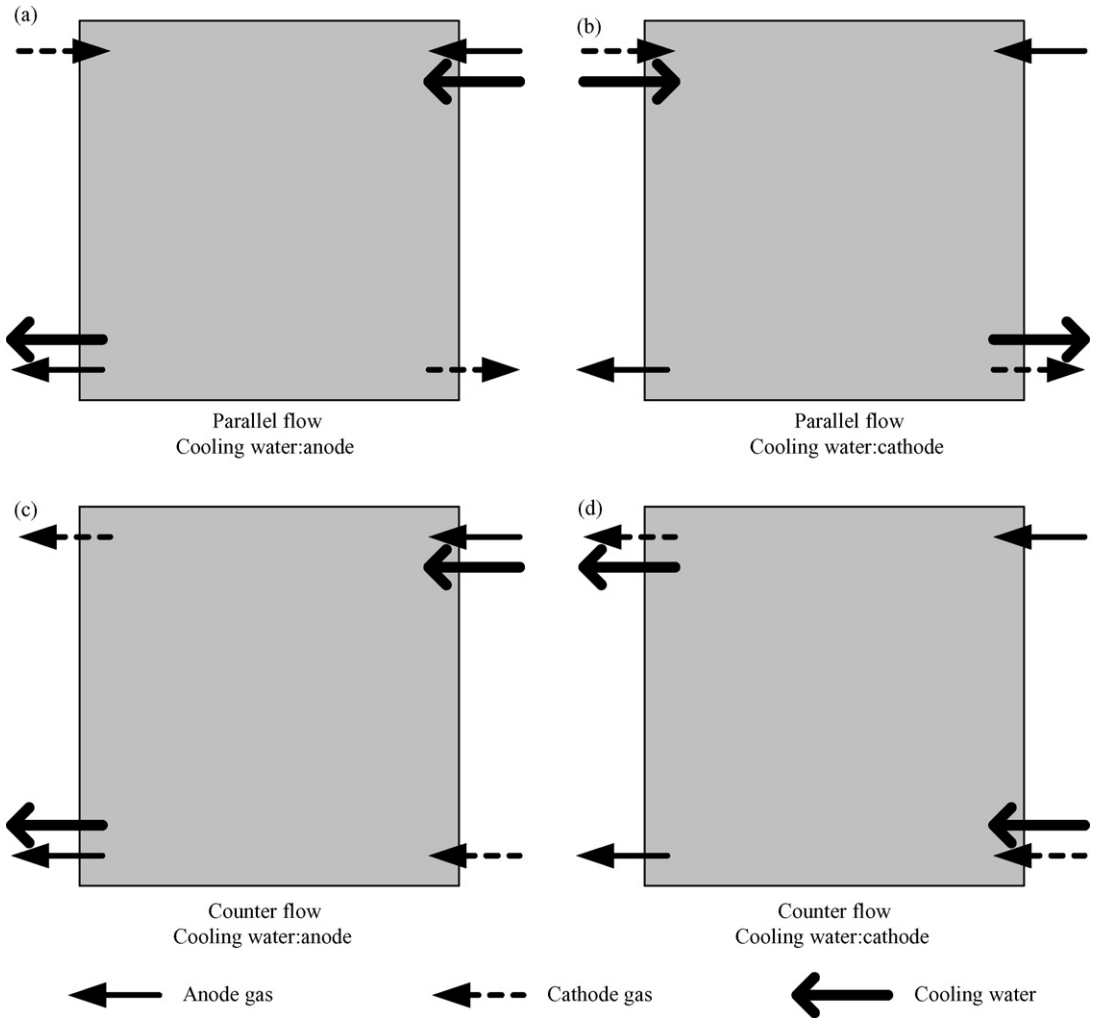

Fig. 4. (a–d) The flow pattern of gas and cooling water.

Table 3
Combination of separator shape and flow pattern

Number	Anode separator	Cathode separator	Flow pattern	Cooling water pattern
1	A	A	Parallel	Anode
2	A	A	Parallel	Cathode
3	A	A	Counter	Anode
4	A	A	Counter	Cathode
5	A	B	Parallel	Anode
6	A	B	Parallel	Cathode
7	A	B	Counter	Anode
8	A	B	Counter	Cathode
9	B	A	Parallel	Anode
10	B	A	Parallel	Cathode
11	B	A	Counter	Anode
12	B	A	Counter	Cathode
13	B	B	Parallel	Anode
14	B	B	Parallel	Cathode
15	B	B	Counter	Anode
16	B	B	Counter	Cathode

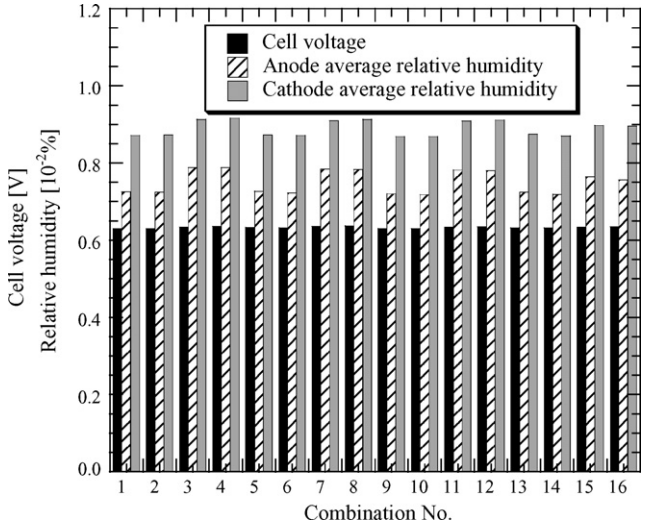

Fig. 5. Calculation results of cell voltage and average relative humidity.

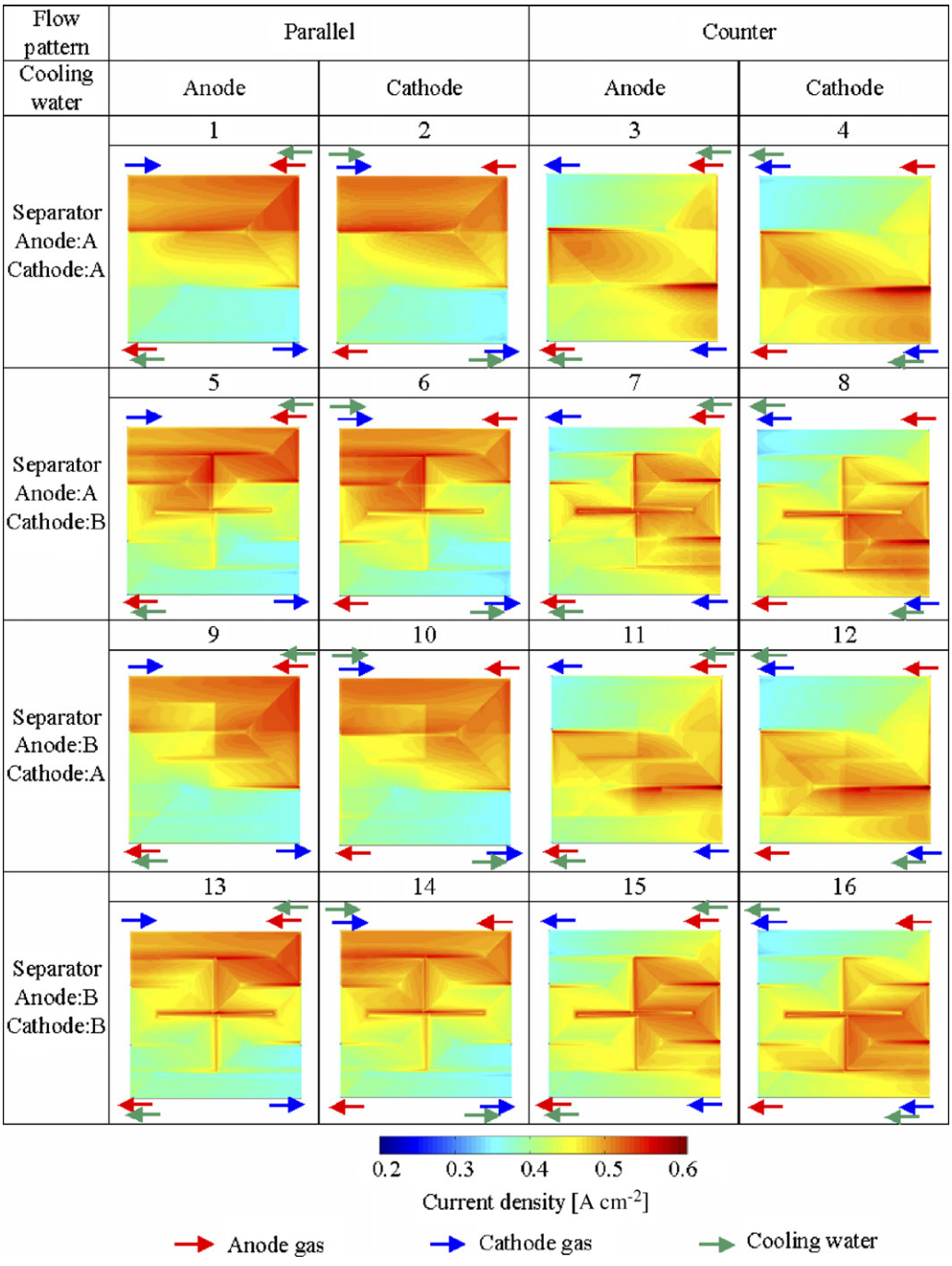

Fig. 6. Current density distribution under each flow condition.

The current density distribution on each condition is shown in Fig. 6. In this figure, the distribution of the parallel gas flow (nos. 1, 2, 5, 6, 9, 10, 13 and 14) was more remarkable than that of the counter gas flow (nos. 3, 4, 7, 8, 11, 12, 15 and 16). It confirms that the influence of the flow pattern of cooling water on the current density distribution was not large. In addition, it was found that the difference of humidity between a right side of the distributed serpentine separator and a left side of it was larger, and that the current density distribution was more uneven when the distributed serpentine separator was used in the cathode channels.

The anode and the cathode relative humidity distribution are shown in Figs. 7 and 8, respectively. In these figures, it could be confirmed that the trend of the humidity distribution in both sides were almost equal to each other. Therefore, it was thought that the humidity distribution in both sides were related to each other by electroosmosis and back-diffusion, and that one did not become more uneven when the other was comparatively uniform. In addition, the humidity distribution of the anode was more remarkable than that of the cathode in each condition, so it was thought that the anode humidity distribution affected the cell durability more.

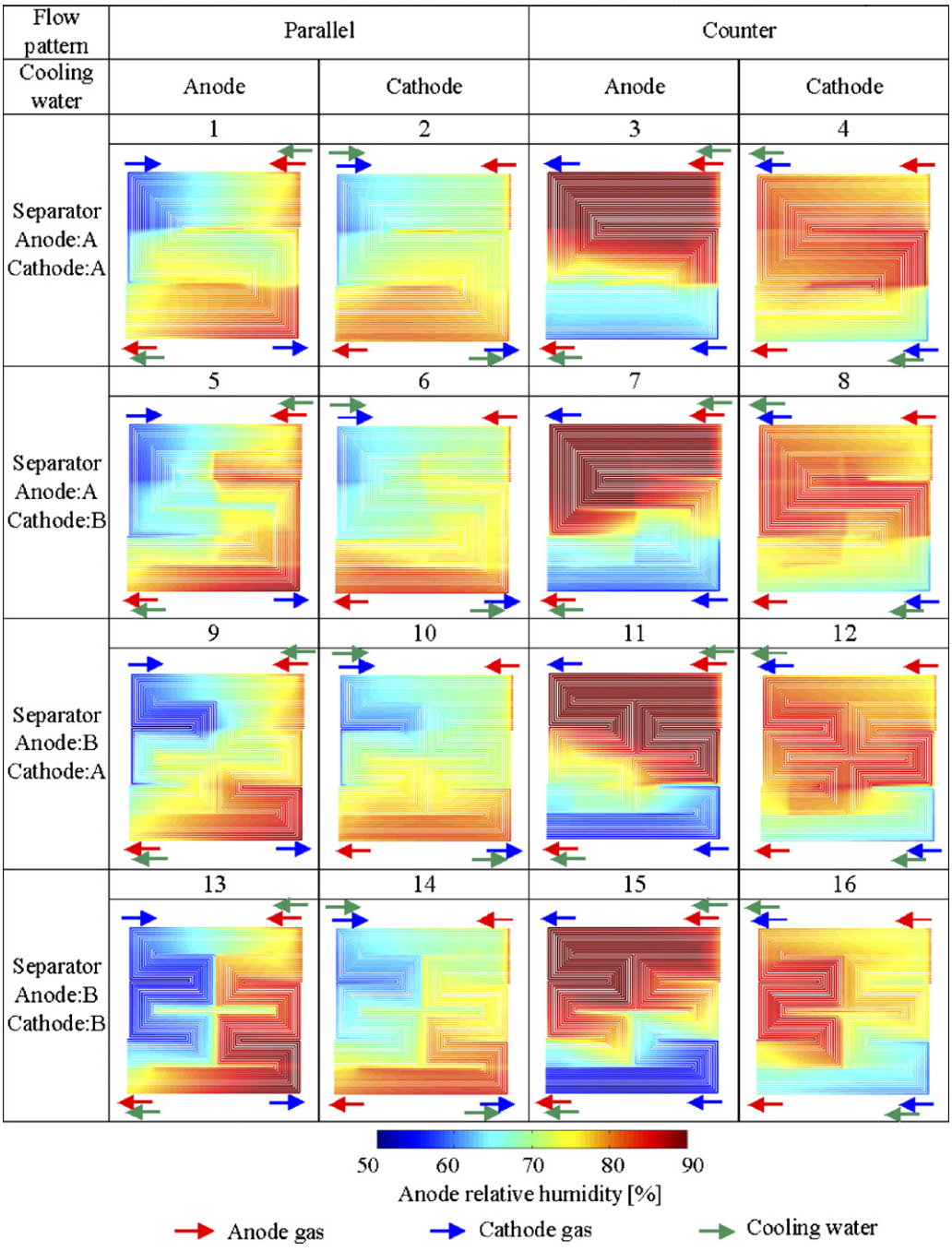

Fig. 7. Anode relative humidity distribution under each flow condition.

Next, the influence of the flow pattern of cooling water on the anode relative humidity distribution was examined. In Fig. 7, when both gases were counter flow and the cooling water was synchronized with the cathode gas, the anode humidity distribution was uniform comparatively. The reasons are thought as follows:

(1) In the upstream area of the anode, the vapor concentration increased because of back-diffusion from the downstream area of the cathode where the vapor concentration was high. And the gas temperature rose because the cooling water was synchronized with the flow of the cathode gas.
(2) In the downstream area of the anode, the vapor concentration decreased because of electroosmosis and the diffusion to the upstream area of the cathode where the vapor concentration was low. And the gas temperature fell because the cooling water was synchronized with the flow of the cathode gas.
(3) The anode vapor concentration and the gas temperature were both high at the upstream area of the anode (1) and these were both low at the downstream area of the anode (2). Con-

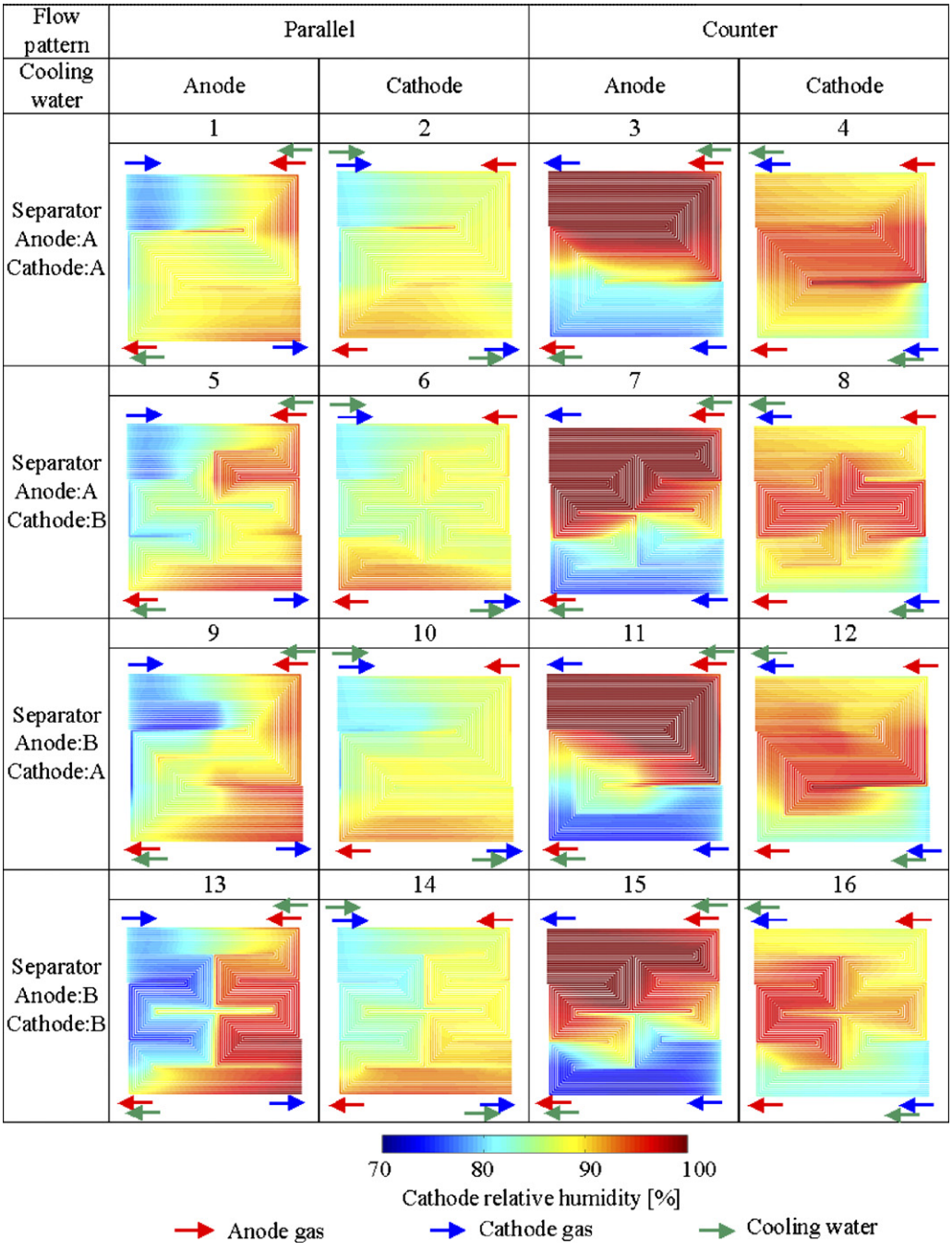

Fig. 8. Cathode relative humidity distribution under each flow condition.

sequently, the relative humidity was uniformly distributed all over the electrode area.

It is also possible to examine the cause of the humidity distribution by investigating the water balance between the anode and the cathode. Next, the influences of channel shapes were examined. The difference of humidity between a right side of the distributed serpentine separator and a left side of it was larger. The unevenness was the largest in particular when the gas flow pattern was parallel and the flow pattern of cooling water was synchronized with the flow of the anode gas (nos. 1, 5, 9 and 13). Whichever the combination was, the relative humidity was lower at the inlet of the cathode, and that was higher at the inlet of the anode under this operating condition. Therefore, the bundle of the gas channels was restricted to the left side (or the right side) of the electrode area because of the distributed serpentine separator, and such uneven distribution was formed.

In order to investigate the current density and humidity distribution quantitatively, the standard deviations of the current density and humidity were calculated. Fig. 9 shows them under each condition. In this figure, it was confirmed that the characters of the anode and the cathode humidity under each condition were the same as each other, and that these characters were not the same as those of the current density. It was thought that

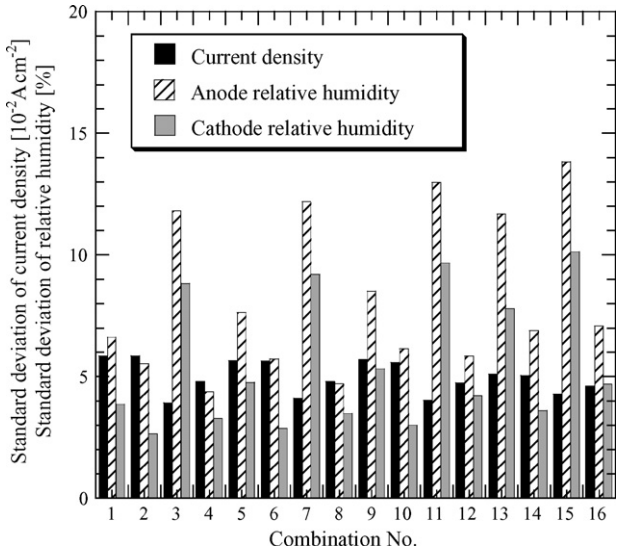

Fig. 9. Standard deviation of current density and relative humidity under each condition.

the uniform current density distribution did not directly relate to the uniform humidity distribution, and that it resulted from that current density distribution was affected by the oxygen concentration and the ionic conductivity which was the function of humidity.

In Fig. 9, the standard deviation of humidity in no. 4 is the lowest. Fig. 10 shows the component ratio of the anode relative humidity distribution on each condition. In this figure, the low humidity area (less than 70%) in no. 4 was smaller than that in other conditions. Although the minimum permissible relative humidity to prevent degradation of membrane cannot be decided because the degradation rate has not been studied, it is expected that the combination of no. 4 can make the relative humidity more uniform and higher, and that this combination improves the cell durability. In addition, as the relative humidity of this combination was less than 90%, it was expected that the effect of the inhibition of the gas flow by liquid water was lower than that of other cases. From the reasons mentioned above, the relative humidity in no. 4 is the highest and the most uniform.

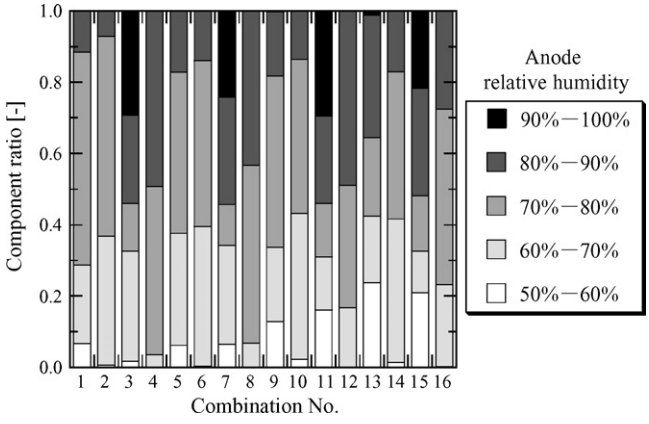

Fig. 10. Component ratio of anode relative humidity distribution.

4. Conclusion

The PEFC reaction and flow analysis model including the effect of heat management by cooling water applied in a PEFC stack was developed. The optimal separator shape and the optimal flow pattern of the gas and the cooling water that make the relative humidity higher and more uniform were examined with this model under each condition. The following results were obtained by these examinations:

1. When the gas flow was counter, the average relative humidity was larger than that of other cases.
2. As the humidity distribution in the anode and the cathode sides were related to each other by electroosmosis and back-diffusion, the trend of the humidity distribution in both sides were almost equal to each other. And the distribution of the anode was more remarkable than that of the cathode in each condition.
3. The uniform current density distribution do not directly relate to the uniform humidity distribution. It resulted from that the current density distribution was affected by the oxygen concentration and the ionic conductivity which was the function of humidity, and that the relative humidity was affected by the generated water and the gas temperature.
4. In the case of the distributed serpentine separator, the difference of humidity between the right side and the left side was larger.

Furthermore, the relative humidity is the highest and the most uniform in the following cases; that the gas flow pattern is counter, that the cooling water is synchronized with the flow of the cathode gas, and that the ordinary serpentine separator is used in the anode and the cathode side. Using the numerical analysis model developed in this study, it is possible to examine the relative the humidity distribution that affects the cell durability and to evaluate the optimal design to control humidity distribution under various operating conditions.

Acknowledgement

This research was supported by the research and development of polymer electrolyte fuel cell from the New Energy and Industrial Technology Development Organization (NEDO), Japan.

References

[1] T.V. Nguyen, R.E. White, A water and heat management model for proton-exchange-membrane fuel cells, J. Electrochem. Soc. 140 (8) (1993) 2178–2186.
[2] J.S. Yi, T.V. Nguyen, An along-the-channel model for proton exchange membrane fuel cells, J. Electrochem. Soc. 145 (4) (1998) 1149–1159.
[3] S. Um, C.Y. Wang, K.S. Chen, Computational fluid dynamics modeling of proton exchange membrane fuel cells, J. Electrochem. Soc. 147 (12) (2000) 4485–4493.
[4] Z.H. Wang, C.Y. Wang, K.S. Chen, Two-phase flow and transport in the air cathode of proton exchange membrane fuel cells, J. Power Sources 94 (2001) 40–50.

[5] S. Dutta, S. Shimpalee, J.W. Van Zee, Three-dimensional numerical simulation of straight channel PEM fuel cells, J. Appl. Electrochem. 30 (2000) 135–146.
[6] T. Berning, D. Lu, N. Djilali, Three-dimensional computational analysis of transport phenomena in a PEM fuel cell, J. Power Sources 106 (2002) 284–294.
[7] S. Um, C.Y. Wang, Three-dimensional analysis of transport and electrochemical reactions in polymer electrolyte fuel cells, J. Power Sources 125 (2004) 40–51.
[8] T. Berning, N. Djilali, Three-dimensional computational analysis of transport phenomena in a PEM fuel cell—a parametric study, J. Power Sources 124 (2003) 440–452.
[9] E. Endoh, S. Honmura, S. Terazono, Degradation study of MEA for PEMFC under low humidity conditions, in: Electrochemical Society's Fall Meeting, Honolulu, October 2004.
[10] C. Zhou, T.A. Zawodzinski, D.A. Schiraldi, Chemical degradation of Nafion^{TM} membranes, in: Electrochemical Society's Fall Meeting, Honolulu, October 2004.
[11] Y. Ikoma, S. Sakamoto, S. Suzuki, M. Karakane, Y. Itoh, K. Takizawa, Study on improvement of durability of polymer electrolyte fuel cell, in: Fuel Cell Seminar, Miami, November 2003.
[12] A.B. LaConti, M. Hamdan, R.C. McDonald, Mechanisms of membrane degradation for PEMFCs, in: W. Vielstich, A. Lamm, H.A. Gasteiger (Eds.), Handbook of Fuel Cells: Fundamentals, Technology, and Applications, vol. 3, Wiley, New York, 2003.
[13] H. Nishikawa, R. Kurihara, S. Sukemori, T. Sugawara, H. Kobayasi, S. Abe, T. Aoki, Y. Ogami, A. Matsunaga, Measurement of humidity and current distribution in a PEFC, J. Power Sources 155 (2006) 213–218.
[14] G. Inoue, Y. Matsukuma, M. Minemoto, Evaluation of the optimal separator shape with reaction and flow analysis of polymer electrolyte fuel cell, J. Power Sources 154 (2006) 18–34.
[15] G. Inoue, Y. Matsukuma, M. Minemoto, Evaluation of the thickness of membrane and gas diffusion layer with simplified two-dimensional reaction and flow analysis of polymer electrolyte fuel cell, J. Power Sources 154 (2006) 8–17.
[16] G. Inoue, Y. Matsukuma, M. Minemoto, Effect of gas channel depth on current density distribution of polymer electrolyte fuel cell by numerical analysis including gas flow through gas diffusion layer, J. Power Sources 157 (2006) 136–152.
[17] G. Inoue, Y. Matsukuma, M. Minemoto, Examination of optimal separator shape of polymer electrolyte fuel cell with numerical analysis including the effect of gas flow through gas diffusion layer, J. Power Sources 157 (2006) 153–165.
[18] H. Dohle, R. Jung, N. Kimiaie, J. Mergel, M. Müller, Interaction between the diffusion layer and the flow field of polymer electrolyte fuel cells—experiments and simulation studies, J. Power Sources 124 (2003) 371–384.
[19] P.H. Oosthuizen, L. Sun, K.B. McAuley, The effect of channel-to-channel gas crossover on the pressure and temperature distribution in PEM fuel cell flow plates, Appl. Therm. Eng. 25 (2005) 1083–1096.